Received: 26 April 2021 | Revised: 6 July 2021 | Accepted: 9 August 2021 | Published on: 19 August 2021

DOI: 10.1002/joc.7338

RESEARCH ARTICLE

International Journal of Climatology RMetS

Asymmetry of daily mean temperature series over China and its frontal mechanism

Heng Quan | **Wenmi Chai** | **Zuntao Fu**

Laboratory for Climate and Ocean-Atmosphere Studies, Department of Atmospheric and Oceanic Sciences, School of Physics, Peking University, Beijing, China

Correspondence
Zuntao Fu, Lab for Climate and Ocean-Atmosphere Studies, Department of Atmospheric and Oceanic Sciences, School of Physics, Peking University, Beijing, China.
Email: fuzt@pku.edu.cn

Funding information
National Natural Science Foundation of China, Grant/Award Numbers: 41475048, 41975059

Abstract

We analyse the European Center for Medium-Range Weather Forecasts reanalysis temperature time series over China and find that daily mean temperature at 850 hPa pressure level warms gradually and cools rapidly, which is known as the asymmetry property. Previous studies pointed out that front events contribute to this asymmetry property, but only presented indirect evidences. Here, we confirm this conjecture with more convincing and direct evidences. The time series of front events are obtained over China by an improved objective front detection algorithm. The high Pearson correlation between time series of monthly temperature asymmetry measure and time series of monthly front events over some specific regions indicates they are closely related to each other and front events indeed contribute to temperature asymmetry. We discover that the North China Plain is a representative region where front events contribute to temperature asymmetry significantly. Further diagnostic analysis by temperature tendency equation shows that the asymmetry of daily mean temperature series is due to the asymmetry between the frequency and intensity (mainly the intensity of meridional nonlinear advection term) of cold and warm fronts in North China Plain.

KEYWORDS

diagnostic analysis, front events, mechanism, temperature asymmetry, time series

1 | INTRODUCTION

The asymmetry property of diversified time series in atmospheric science, which is one of the fundamental features of weather and climate variations on Earth, has been confirmed in lots of previous studies, on time scales from millions of years to days. For example, glaciation phases lasted longer than deglaciation phases during mid-Pleistocene cycles (Tziperman and Gildor, 2003), El Niño events have greater amplitude than La Niña events (Burgers and Stephenson, 1999; Su *et al*., 2010) and zonal asymmetry exists in both background state and forcing in the Madden–Julian oscillation and sudden stratospheric warming teleconnection mechanism (Kang and Tziperman, 2018).

The asymmetry property of time series often implies nonlinear underlying dynamics (Bartos and Jánosi, 2005; Lacasa *et al*., 2012); hence, studies on it can help us to better understand nonlinear interactions among physical processes. In this study, we focus on temporal asymmetry. For a given process x_t, if the statistical features of time series x_t in original and reversed order are significantly different, then, x_t is temporal asymmetric (Weiss, 1975).

Previous studies (Bartos and Jánosi, 2005; Gyüre *et al*., 2007; Ashkenazy *et al*., 2008) have discovered that the asymmetry property of daily mean temperature series, which cools rapidly while warms gradually, is a common phenomenon at the mid-latitudes. Recent studies (Xie *et al*., 2016) on station measurements also confirm that

such behaviour can be identified in most parts of China. The distribution of temperature asymmetry (based on the European Center for Medium-Range Weather Forecasts [ECMWF] reanalysis, European Center for Medium-Range Weather Forecasts reanalysis (ERA) for short) is shown in Figure 1. It has been thought that such temperature asymmetry is mainly due to front events (Ashkenazy *et al*., 2008; Piskala and Huth, 2020).

Ashkenazy *et al*. (2008) discovered that the intensity of temperature asymmetry decreases when the time lag of the series increases or the altitude rises, and almost disappears at 500 hPa level or with time lag $\tau = 7$ days at the mid-latitudes. The highest altitude of front events is about 4.5 km (Trewartha, 1954) and frontal zones are unusual at 500 hPa level (Wallace and Hobbs, 2006). Moreover, the time scale of temperature asymmetry approximately equals to the time scale of front events (within 1 week) (Ashkenazy *et al*., 2008). Therefore, the synoptic temporal and spatial scale of temperature asymmetry is similar to the synoptic temporal and spatial scale of front events. However, these are only indirect evidences proving that front events contribute to temperature asymmetry.

Statistics also showed that strong day-to-day temperature variations are often accompanied by front events at the Praha–Karlov station (where front passage is recorded) (Piskala and Huth, 2020), which also implies that front events contribute to temperature asymmetry, but only deals with relative percentages at a single station rather than doing a regional diagnostic analysis.

Do front events contribute to daily mean temperature asymmetry in a given region? How can we find regions where front events contribute to temperature asymmetry significantly? How do front events affect temperature asymmetry in such regions? These questions have not been answered well so far, and they are what we want to solve in this study, with the help of the objective front detection algorithm.

It should be pointed out that the studies on temperature asymmetry are of great importance. They not only deepen our understanding about nonlinear interactions among physical processes and features of extreme events, but also benefit studies on other fields like health issues. For example, some previous studies (Guo *et al*., 2011; Cheng *et al*., 2014, 2016; Vicedo-Cabrera *et al*., 2015; Zhan *et al*., 2017) discovered that strong temperature variation between adjacent days can significantly increase mortality and the chances of some diseases. Studying the mechanism of temperature asymmetry, especially the mechanism of asymmetry between strong temperature increases and decreases, can help us to better evaluate the chances of diseases through a dynamical prospective.

The rest of the paper is organized in the following order. In Section 2.1, we will briefly describe the data used in this paper. The measure of daily mean temperature asymmetry that we used and the improved objective front detection algorithm are presented in Sections 2.2 and 2.3, respectively. Section 3 shows our major results, including the identification of the representative region

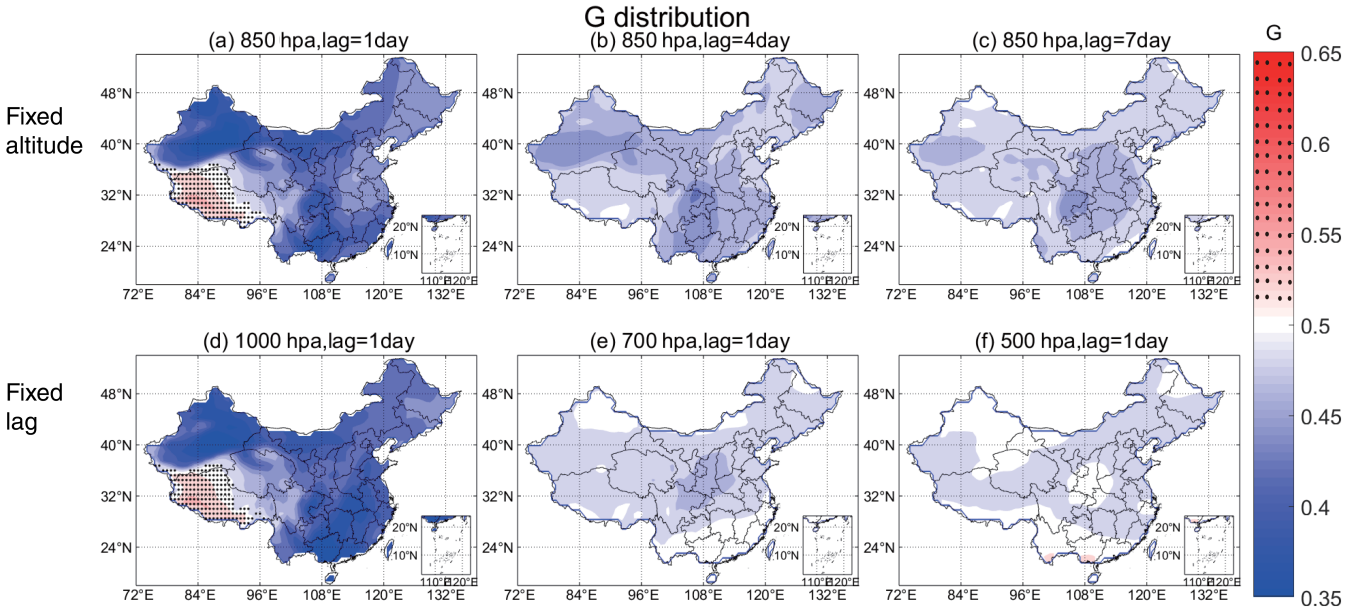

FIGURE 1 The distribution of asymmetry measure G over China, based on daily mean temperature series with different lags at different pressure levels. (a–c) 850 hPa, lag $\tau = 1, 4, 7$ days; (d–f) 1,000, 700, 500 hPa, lag $\tau = 1$ day [Colour figure can be viewed at wileyonlinelibrary.com]

where fronts contribute to temperature asymmetry significantly, by means of conditional mean approach and Pearson correlation in Section 3.1; and the diagnostic analysis about how fronts contribute to temperature asymmetry in Section 3.2. Finally, in Section 4, conclusions and further discussions are made.

2 | DATA AND METHODS

2.1 | Data

The dataset used in this article is from the ECMWF. More specifically, we analyse its ERA-Interim dataset (Dee *et al*., 2011). (We have repeated our study on the ERA5 dataset and found that our results are quite similar between them. The figures are not shown here.) The length of the series is 40 years, from 1979 to 2018. The region we concern covers inland China inside, which is from 3° to 54°N, 72° to 138°E. The temporal resolution is 6 hours, while the spatial resolution is 0.75°.

In this study, we use daily mean data unless specifically emphasized. It is achieved by simply calculating the arithmetic mean of four consecutive instantaneous values (at 0:00, 6:00, 12:00, 18:00, respectively) in the same day.

Following (Jenkner *et al*., 2010), a simple diffusive smoothing procedure is applied to all variables and their four direct neighbours to reduce the spatial noise of high-resolution data and emphasize the feature of regions rather than grid points:

$$\tau_{i,j}^{n}=\frac{1}{2}\tau_{i,j}^{n-1}+\frac{1}{8}\left(\tau_{i+1,j}^{n-1}+\tau_{i-1,j}^{n-1}+\tau_{i,j+1}^{n-1}+\tau_{i,j-1}^{n-1}\right),n=1,2,...,n_f \quad (1)$$

The round of smoothing, n_f, is set to be 15, which is considered suitable for China after thorough tests.

2.2 | Asymmetry measure of temperature series

Up to now, various measures of the temporal asymmetry property have been developed, as reviewed in the recent comparison study (Zhang *et al*., 2019). Some of those measures include a symbolization process and then analyse the difference between the enciphered string in original and reversed order (Daw *et al*., 2000), but they are considered biased due to extra subjective arguments (Lacasa *et al*., 2012). Therefore, measures without the symbolization procedure are more objective and accurate, like measures derived from directed horizontal visibility graph (DHVG) (Luque *et al*., 2009; Lacasa *et al*., 2012) and consecutive increasing and decreasing steps (CIDS) (Xie *et al*., 2016). These two measures and the other three measures listed below reach quite a consistent results when measuring the asymmetry of daily mean temperature series (Zhang *et al*., 2019).

The measure we choose in this study is related to the increments of series. The increment time series Δx_i of a series x_i is $x_{i+\tau}-x_i$, given a specific lag τ ($\tau=1$ by default unless specifically emphasized in this study). There are three commonly used asymmetry measures, named A (Ashkenazy *et al*., 2008), E (Ehlers *et al*., 1998), and G (Guzik *et al*., 2006) respectively, based on the increment series:

$$A=\frac{\sum_i\theta(\Delta x_i)}{\sum_i\theta(\Delta x_i)+\sum_i\theta(-\Delta x_i)}, \quad (2)$$

$$E=\frac{\sum_i(\Delta x_i)^3}{\left[\sum_i(\Delta x_i)^2\right]^{3/2}}, \quad (3)$$

$$G=\frac{\sum_i(\Delta x_i\cdot\theta(\Delta x_i))^2}{\sum_i(\Delta x_i)^2}, \quad (4)$$

where $\theta(x)=1$ for $x>0$ and zero elsewhere.

Obviously, the measure A only takes the signs of consecutive increments Δx_i into account, while E and G consider both the signs and magnitude of Δx_i.

For a 40-year-long daily mean temperature series, when the temperature cools rapidly and warms gradually (hence decrease is less frequent than increase), as commonly found at the mid-latitudes, $A>0.5$. If A 0.5, then the series is temporal symmetric. The closer A is to 0.5, the more temporal symmetric the series is. Similarly, when G 0.5 or E 0, then the series is temporal symmetric. $A>0.5$ usually accompanies $G<0.5$ and $E<0$.

We choose measure G as the measure of asymmetry in this study. We find that the results from these three measures are quite similar (the figures are not shown here). We evaluate the intensity or significance of the asymmetry property of a given time series by surrogate method. More specifically, we randomly exchange two values in the series for many (e.g., the length of the series) times to get one surrogate series, and repeat this procedure for 1,000 times to get 1,000 surrogate series. For each of these 1,000 surrogate series, we calculate its asymmetry measure G and sort the 1,000 values from the smallest to the biggest. The 25th and 975th values in this series constitute an interval. If the original series' G measure lies out of the interval, then the null hypothesis that the original series is temporal symmetric is rejected, with a significant p-value less than .05.

Here, we calculate the measure G of the 40-year-long daily mean temperature series at each grid point in China with different lags ($\tau = 1$, 4 and 7 days) at different pressure levels (1,000, 850, 700 and 500 hPa). The distribution of measure G is shown in Figure 1.

Figure 1 clearly shows that the intensity of temperature asymmetry decreases when the lag increases or the altitude rises, and almost disappears at 500 hPa level or with lag $\tau = 7$ days, which is consistent with previous results given for Northern hemisphere (Ashkenazy *et al.*, 2008). Also, daily mean temperature at 1,000 and 850 hPa levels share similar spatial patterns with gradual warming and rapid cooling (since $G < 0.5$) in most parts of China (except the Tibetan Plateau), and this asymmetry property is stronger over southeast and northwest of China, which agrees with results based on station measurements (Xie *et al.*, 2016).

2.3 | Objective front detection algorithm

Synoptic-scale fronts are very important to weather in the mid-latitudes. Previous studies show that front events are not only related to extreme weather like heavy rains and extreme winds (Catto *et al.*, 2012; Catto and Pfahl, 2013), but also concurrent with other weather systems like cyclones and thunderstorms (Dowdy and Catto, 2017). In this study, we want to relate front events to day-to-day temperature variability and its asymmetry property in inland China, with the help of the objective front detection algorithm.

The objective front detection algorithm is a method to objectively detect frontal regions in a given area at a certain moment and pressure level, using data from a reanalysis dataset. More specifically, for each grid point in a given region, we detect whether there is a front event at that grid point; if the answer is yes, we should identify whether it is a cold or warm front (more complicated types of fronts ignored). Contiguous grid points with the same kind of front constitute a frontal zone.

The objective front detection algorithm was first invented in 1965 (Renard and Clarke, 1965), and has been revised for many times (Huber-Pock and Kress, 1989; Steinacker, 1992; Hewson, 1998; Mccann and Whistler, 2001; Jenkner *et al.*, 2010; Berry *et al.*, 2011; Schemm *et al.*, 2015). Traditional methods mentioned above mainly identify fronts by checking several criteria from a thermal perspective, while recently deep learning is applied to improve the accuracy of objective front detection (Lagerquist *et al.*, 2019). Now the objective front detection algorithm is accurate and quite consistent with subjective analyses. Here, we improve the traditional algorithm to adapt to front detection in inland China.

As most traditional objective front detection algorithms do, we first calculate the thermal front parameter (TFP) for each grid point, which was first described in (Renard and Clarke, 1965). The definition of TFP is:

$$\mathrm{TFP}(T) = -\nabla|\nabla T|\frac{\nabla T}{|\nabla T|}, \tag{5}$$

where T is temperature. Notice that some studies used other variables (like potential temperature) instead of temperature itself, but reached similar results (Hewson, 1998).

TFP is used to locate potential frontal zones. It represents the gradient of the magnitude of the gradient of a thermodynamic scalar quantity, resolved into the direction of the gradient of that quantity (Renard and Clarke, 1965). At first, Clarke indicated that TFP's ridgelines (or maxima) are where front events probably lie, while a later research showed that the zero contours of TFP field are potential locations of fronts (Jenkner *et al.*, 2010). Here, we follow the latter approach.

In practice, if

$$\mathrm{TFP}(T) < K_1, \tag{6}$$

we consider probably that there is a front at that grid point. By this way, we get the potential frontal zones.

Next, we apply masking criteria to eliminate spurious grid points in the potential frontal zones obtained above. Only if all the masking criteria are satisfied can the grid point be truly considered with the front at that moment.

The first masking criterion is:

$$|\nabla T| > K_2 \tag{7}$$

This is because temperature often changes steeply in frontal regions.

The second masking criterion is:

$$\left|\vec{v}\cdot\frac{\nabla T}{|\nabla T|}\right| > K_3 > 0, \tag{8}$$

where $\vec{v}$ is horizontal wind velocity. This is because frontal zones often have intense horizontal thermal advection. $\vec{v}\cdot\frac{\nabla T}{|\nabla T|} > K_3$ means cold front (because wind heads toward warmer place), while $\vec{v}\cdot\frac{\nabla T}{|\nabla T|} < -K_3$ means warm front.

After thorough tests, the arguments suitable for China are: $K_1 = 0.00005\ \mathrm{K}\cdot\ \mathrm{km}^{-2}$, $K_2 = 0.016\ \mathrm{K}\cdot\mathrm{k\ m}^{-1}$, $K_3 = 5\ \mathrm{m}\cdot\ \mathrm{s}^{-1}$. Changing the thresholds slightly will bring slight changes to the frequency of cold and warm fronts, but will not affect their relative frequency and

intensity. Therefore, our results are quite robust and not sensitive to the thresholds in front detection algorithm. Remember all variables have gone through the smoothing procedure in Section 2.1.

The choice of the pressure level is an important feature of the detection algorithm. Different previous detection algorithms work at different pressure levels, which are reviewed in (Hewson, 1998). In our study, we choose 850 hPa pressure levels. On the surface, orography brings extra noise, especially given that China has very complex terrain; on higher pressure levels (e.g., 700 or 500 hPa) gradients of thermal variables are relatively small, hence, our detection algorithm will not work.

Now, we illustrate this algorithm in Figure 2. It shows the distribution of frontal zones (Figure 2a) and the three criteria mentioned above (Figure 2b–d) on 21 November, 2020, at 0600 UTC. We successfully identify the cold front event occurring then.

Our improved objective front detection algorithm is not only accurate (ensured by comparison with manual weather maps from the National Meteorological Center in China, for example, our Figure 2a successfully detect the cold front event shown in Figure 3), but also easier and more convenient than previous algorithms.

3 | RESULTS

3.1 | Regions where front events contribute to temperature asymmetry significantly

Applying the improved objective front detection algorithm, we can easily judge whether there is a front, and whether it is a warm or cold front, in a certain day at a given grid point. Since we want to calculate daily mean temperature tendency in days with cold and warm front and evaluate how they contribute to daily mean temperature change, we ignore a few complicated days (less than 1%) with the both cold and warm front passage at

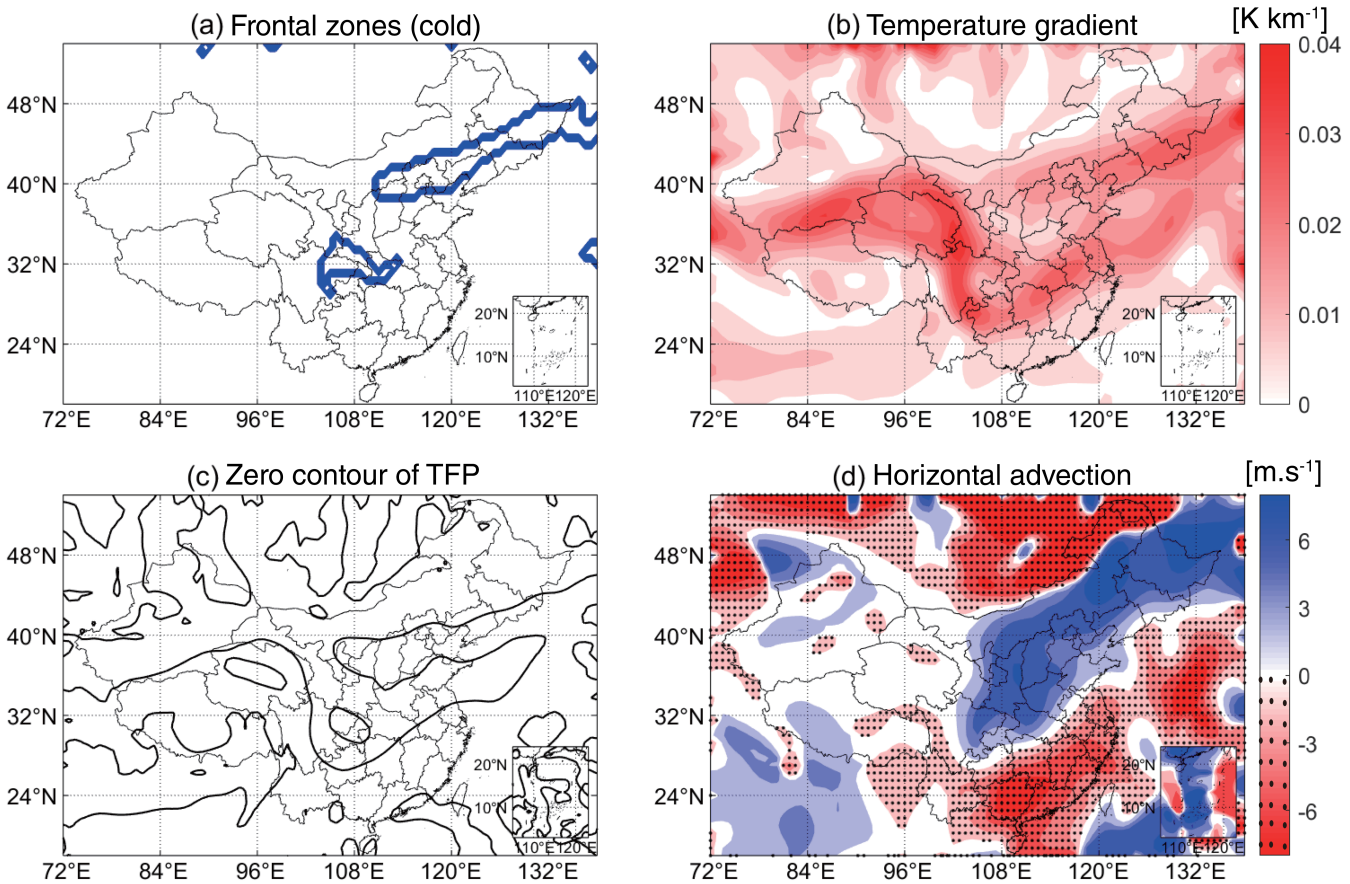

FIGURE 2 The process of objective front detection algorithm for a typical case on 21 November, 2020, 0600 UTC, 850 hPa pressure level. (a) Grid points meeting the three criteria constitute frontal zones. Here, only cold frontal zones (enclosed in solid thick lines) exist; (b) distribution of the magnitude of temperature gradient. Criterion: $|\nabla T| > 0.016\ \mathrm{K \cdot km^{-1}}$ (Eq. (7)); (c) zero contour of TFP. Criterion: $|TFP| < 0.00005\ \mathrm{K \cdot km^{-2}}$ (Eq. (6)); (d) distribution of horizontal wind velocity's projection to the direction of temperature gradient. Criterion: $\left|\vec{v}\frac{\nabla T}{|\nabla T|}\right| > 5\ \mathrm{m \cdot s^{-1}}$ (eq. (8)) [Colour figure can be viewed at wileyonlinelibrary.com]

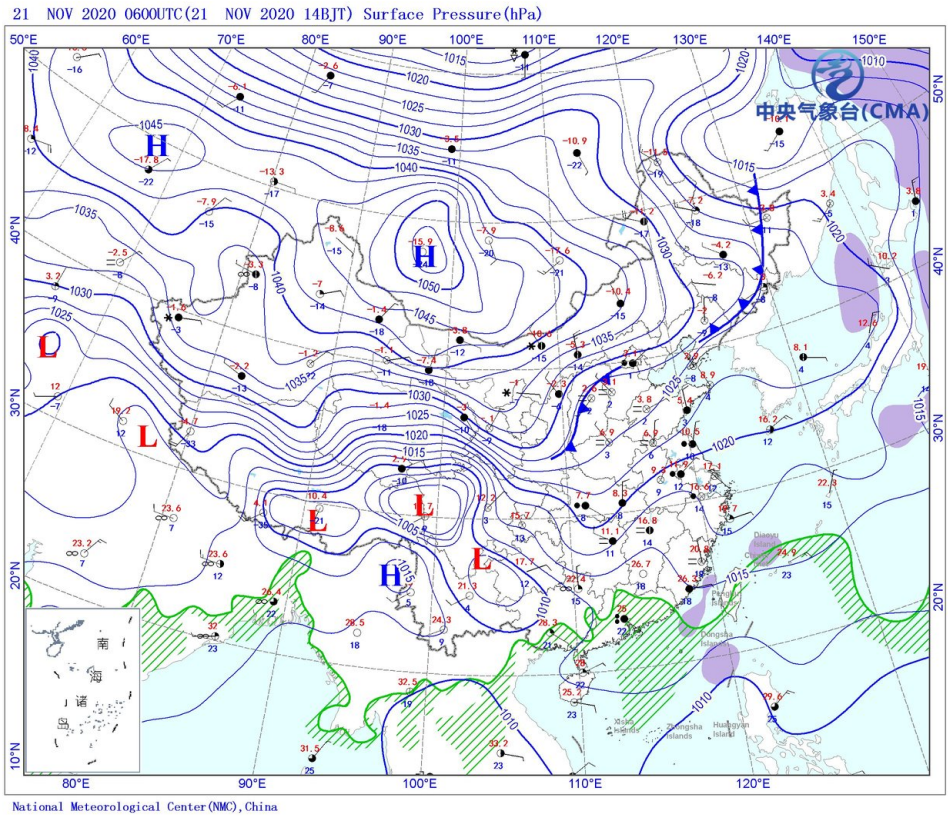

FIGURE 3 (21 November, 2020, 0600 UTC) Manual front detection result. The solid thick line with triangles represents a cold front. This figure is from National Meteorological Center in China [Colour figure can be viewed at wileyonlinelibrary.com]

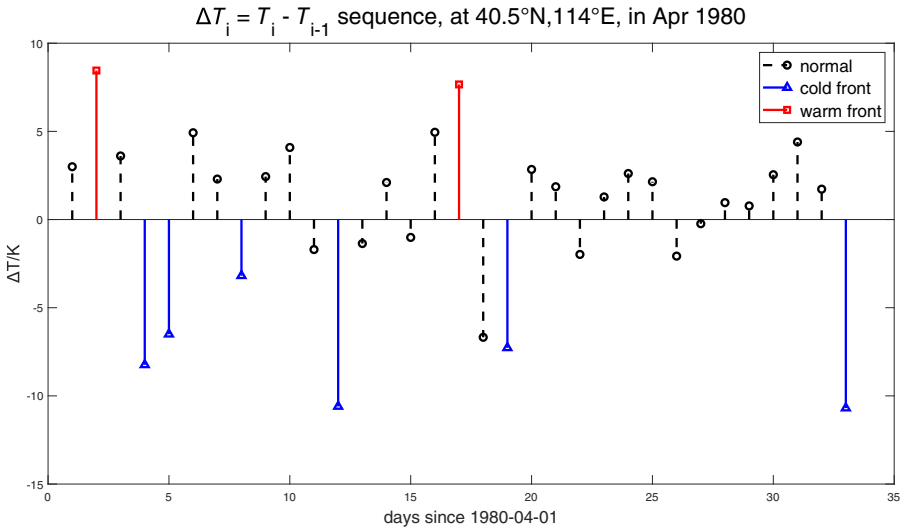

FIGURE 4 Temperature increment series $\Delta T_i = T_{i+1} - T_i$, at 114°E, 40.5°N, in Apr 1980. Lines with solid suares (warm) and triangles (cold) represent day-to-day temperature changes accompanied by front events, identified by our improved objective front detection algorithm [Colour figure can be viewed at wileyonlinelibrary.com]

different moments. (If there are both cold and warm fronts in a day, we cannot tell whether that day's temperature change is caused by cold or warm front.) Figure 4 is an example showing the result of our front detection algorithm at 114°E, 40.5°N in some days, and it makes sense that front events accompany strong temperature changes. For each grid point, we can easily get its time series of 40-year-long daily front events and calculate its 40-year-average annual and monthly front frequency.

First, we calculate the frequency distribution of front events over China (measured by the number of days with front events per year on average), see Figure 5. From Figure 5, we can learn that cold fronts are frequent over northeast and northwest of China, while warm fronts are frequent over northeast and middle-south of China. The metric bars also indicate that cold fronts are more frequent than warm fronts in most parts of China. It should be pointed out that the 850 hPa pressure level is below the surface in the Himalayan region and wind velocity

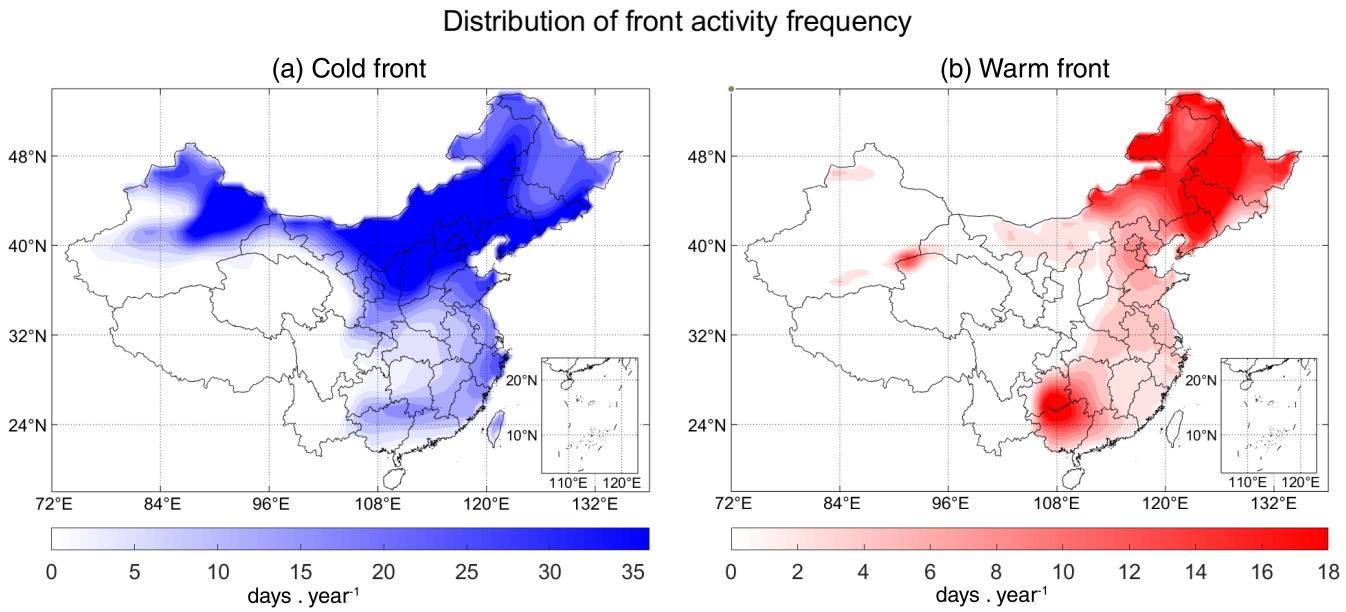

FIGURE 5 The frequency distribution of front events over China, measured by days per year with (a) cold fronts; (b) warm fronts on average [Colour figure can be viewed at wileyonlinelibrary.com]

below the surface is generated by extrapolation, so front detection results are meaningless there. Therefore, we simply ignore this region. (If we do not mask Himalayan region, it only has no more than four front events in 40 years, which is neglectable.)

Our results in Figure 5 are in agreement with a previous study focusing on objective front detection in inland China (Zhou, 2018). Zhou also used ERA-Interim data from 1979 to 2018. We preprocessed the data and present our front climatology results in similar way as Zhou did. He and our study used different front detection criteria but reach similar results (Figure 5 is quite similar to figures 3.9 and 3.12 of Zhou (2018)).

Next, we test whether front events contribute to temperature asymmetry in a given region by two methods.

The first method is the conditional mean approach (Jajcay *et al*., 2016). We apply Fourier transform to the time series of 40-year-long monthly front frequency (480 points) at each grid point over China, and find that most of them have a significant 12-month long period. For each grid point, we calculate the 40-year-average asymmetry measures G in 12 months (corresponding to 12 phases in front frequency cycles). Figure 6a shows the monthly mean G series at 114E, 40.5°N. If front events do not influence temperature asymmetry, the 12 conditional means would approximately be the same.

Then, we test whether the maximum and minimum values among the 12 conditional means are significantly different. By shuffling method (similar to Section 2.2) we get 1,000 surrogate monthly G series (480-point-long), and calculate the range of monthly mean G series (12-point-long) for each one. In Figure 6b, we present the histogram of the 1,000 ranges at 114°E, 40.5°N. The thick dash line in Figure 6b corresponds to a range larger than the thick solid line, showing that the maximum and minimum values among 12 conditional means in Figure 6a are significantly different, with a *p*-value smaller than .05. Therefore, front events do influence temperature asymmetry significantly at 114°E, 40.5°N. This test can be easily repeated at other grid points.

The second method is to evaluate the correlation between front events and temperature asymmetry. For each grid point, we calculate its 40-year-average asymmetry measures (as described in Section 2.2) of daily mean temperature series for each month and get a 12-point-long monthly G time series (like Figure 6a at 114°E, 40.5°N). Similarly, we calculate its 40-year-average days with the front in each month and get a time series of monthly mean front frequency (like Figure 6c at 114°E, 40.5°N). The Pearson correlation between the two 12-point-long series is obtained (like the thick dash line in Figure 6d at 114°E, 40.5°N), which measures the intensity of correlation between front events and asymmetry of daily mean temperature series at this grid point.

Since $G < 0.5$ almost everywhere over China (see Figure 1), the smaller G is, the more intense the asymmetry feature is. So, if the valleys of G series are accompanied by the peaks of the front frequency time series and the former's valleys are accompanied by the latter's

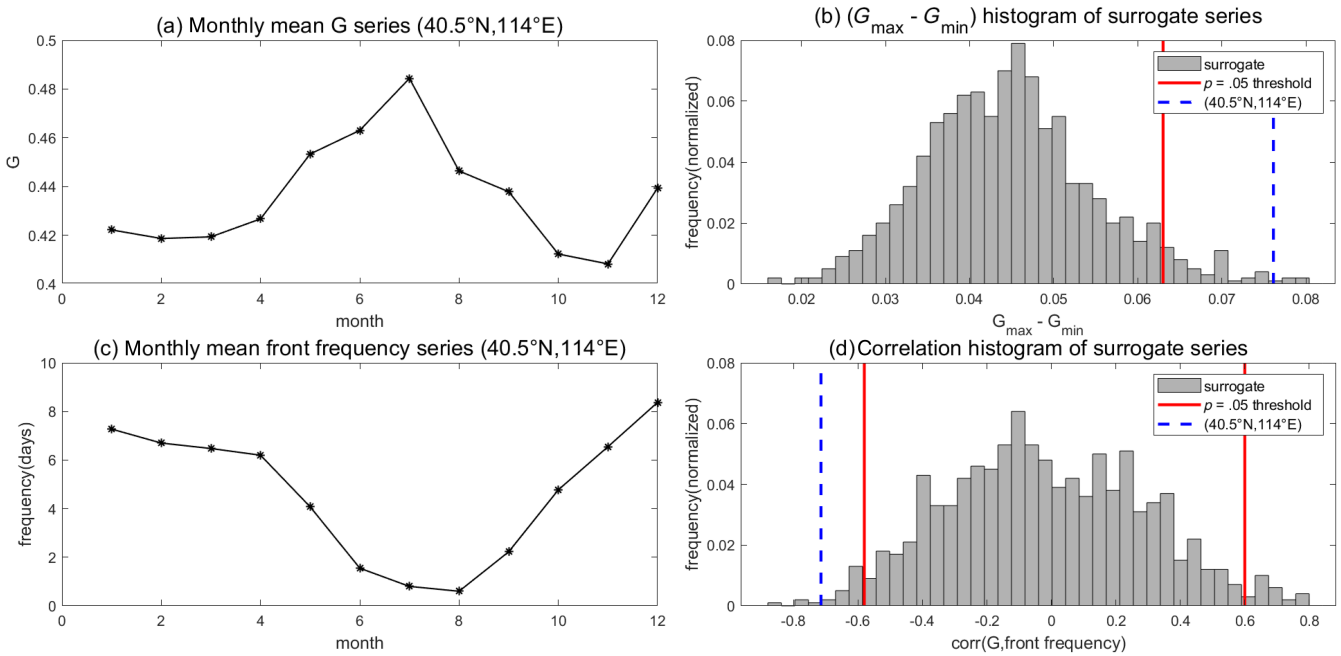

FIGURE 6 (a) Monthly mean time series of temperature asymmetry measure G at 114°E, 40.5°N; (b) the histogram of the ranges of 1,000 surrogate monthly mean G series at 114°E, 40.5°N. The thick solid line represents the 50th biggest range, which is also the $p = .05$ threshold. The thick dash line is the range of monthly mean G series at 114°E, 40.5°N in (a); (c) monthly mean time series of front events frequency at 114°E, 40.5°N; (d) the histogram of the Pearson correlations between the 1,000 surrogate monthly mean G series and the original monthly mean front frequency series in (c) at 114°E, 40.5°N. The two thick solid lines represents the 25th biggest and 25th smallest value among the 1,000 correlations, which are also the $p = .05$ thresholds. The thick dash line represents the Pearson correlation between the original monthly mean G series in (a) and the original monthly mean front frequency series in (c) at 114°E, 40.5°N [Colour figure can be viewed at wileyonlinelibrary.com]

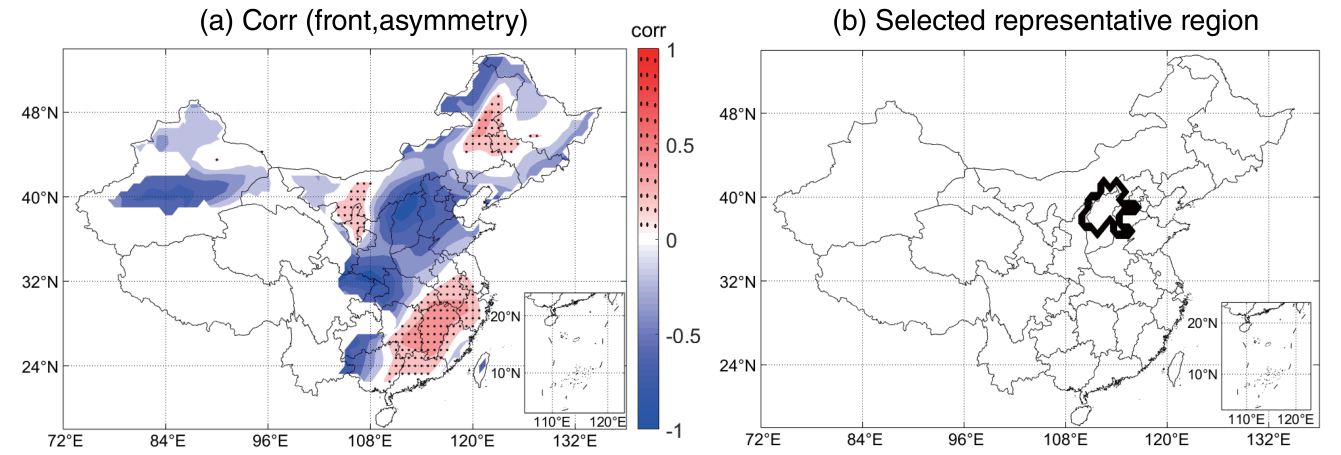

FIGURE 7 (a) Distribution of the Pearson correlation between monthly front frequency time series and monthly temperature asymmetry time series. Dark shading areas without dots (correlation close to −1) are where we consider front events are likely to contribute to temperature asymmetry; (b) the representative region in North China plain for further diagnostic study, selected by criteria in text [Colour figure can be viewed at wileyonlinelibrary.com]

peaks, then, intense temperature asymmetry is accompanied by frequent front events. Therefore, the closer the correlation is to −1, the more likely front events contribute to temperature asymmetry.

Figure 7a shows the distribution of the Pearson correlation between front events and temperature asymmetry. Dark shading areas without dots (correlation close to −1) in Figure 7a, like the North China Plain, Xinjiang

Province and some regions in the south of China, are where we consider front events are likely to contribute to temperature asymmetry.

To test the significance of the Pearson correlation between front frequency series and G series, we use the surrogate method similar to Section 2.2. We apply the shuffling procedure to G series for 1,000 times and get 1,000 surrogate series. For each, we calculate the Pearson correlation between it and the front frequency time series, sort the 1,000 correlations in order (like the histogram in Figure 6d at 114°E, 40.5°N), in which the 25th biggest and smallest value constitute an interval (like the interval between the two thick solid lines in Figure 6d at 114°E, 40.5°N). If the original correlation (like the thick dash line in Figure 6d at 114°E, 40.5°N) exceeds this interval, the null hypothesis that the two series are not related is rejected, with a significant p-value less than 0.05. In those regions that the two series are significantly and negatively correlated, we consider front events contribute to temperature asymmetry significantly.

Now, we select representative grid points for further diagnostic study, based on the following criteria:

1. Fronts influence temperature asymmetry significantly (confirmed by the conditional mean test, $p = .05$);
2. correlation in Figure 7a is significant and negative;
3. significant asymmetry measure G, as described in Section 2.2;
4. more than 8 days with cold front per year on average;
5. more than 2 days with warm front per year on average.

The arguments in the last two criteria are somewhat subjective, but our results depend only slightly on them.

Grid points (34 in total) meeting these criteria constitute the region enclosed by the thick solid line in Figure 7b. It is a part of the North China Plain.

If we remove days with front events and calculate the asymmetry measure G of the rest of the days without front events, the asymmetric feature that temperature warms gradually and cools rapidly will reverse (turn from $G < 0.5$ originally to $G > 0.5$) in the representative region. For example, we focus on the grid point at 114°E, 40.5°N, with $G = 0.423$ (significant). If we remove all the temperature changes with front events in 40 years in Figure 4 (solid lines with squares and triangles), then $G = 0.605$ (significant) for the remaining temperature changes without front events (dash lines with circles) in 40 years. This ensures that front events do contribute to the asymmetry of strong temperature changes (as it is shown in Figure 4, strong temperature changes are often accompanied by front events). Also, there must be processes other than front events that have opposite impacts on the asymmetry of weak temperature changes.

3.2 | Diagnostic analysis: How do front events contribute to temperature asymmetry?

Now, we analyse how front events contribute to temperature asymmetry in the representative region in North China Plain.

Since $G < 0.5$ means that temperature warms gradually and cools rapidly, it is natural to guess that cold fronts are stronger than warm fronts, or in other words, cold fronts cause severe cooling while warm fronts cause mild warming. Actually, our results in Figure 8 confirm this hypothesis. There are several factors contributing to temperature change, like advection and radiation. What is the dominant factor making cold fronts stronger than warm fronts?

We refer to the temperature tendency equation commonly used in El Niño and Indian Ocean Dipole studies (Li *et al.*, 2002; An and Jin, 2004; Hong *et al.*, 2008a, 2008b; Su *et al.*, 2010):

$$\frac{\partial T}{\partial t} = -v \cdot \nabla T + \left(-\omega \frac{\partial T}{\partial p} + \omega \frac{\kappa T}{p} \right) + \frac{J}{c_p} + R \qquad (9)$$

This equation is simply derived from the first law of thermodynamics. When we analyse the factors contributing to daily temperature's tendency at 850 hPa pressure level, $\vec{v}$ represents horizontal wind velocity, $-\vec{v} \cdot \nabla T$ is the horizontal advection term, $-\omega \frac{\partial T}{\partial p}$ is vertical advection term, $\omega \frac{\kappa T}{p}$ is the adiabatic expansion term where $\kappa = \frac{R_d}{c_p}$. We add the two terms involving vertical velocity ω together to get the vertical term $\left(-\omega \frac{\partial T}{\partial p} + \omega \frac{\kappa T}{p} \right)$. $\frac{J}{c_p}$ is the diabatic heating term (including sensible heat flux, latent heat flux, shortwave radiation and longwave radiation) and R is the residue term.

The advection term can also be decomposed:

$$\vec{v} \cdot \nabla T = \overline{\vec{v}} \cdot \nabla \overline{T} + \left(\overline{\vec{v}} \cdot \nabla T' + \overline{\vec{v'}} \cdot \nabla \overline{T} \right) + \overline{\vec{v'}} \cdot \nabla T' \qquad (10)$$

where $\overline{(\ )}$ represents climatological annual cycle (CAC) and $(')$ represents anomaly. The three terms on the right-hand side of Eq. (10) are denoted as CAC, linear and nonlinear advection terms, respectively.

For each grid point in the representative region, we first calculate its average daily mean temperature tendency in days with cold fronts and warm fronts (like the solid lines with squares and triangles in Figure 4), and then calculate the mean value of the tendency among all such grid points. Next, we decompose the tendency by Eqs. 9 and 10 to evaluate the contribution of each term.

Figure 8 shows different terms contributing to temperature tendency in days with cold and warm fronts in the representative region in North China Plain.

From Figure 8, we know the following:

1. Average temperature tendency $\frac{\partial T}{\partial t}$ in days with cold fronts is larger than in days with warm fronts. Cold fronts let temperature cool rapidly while warm fronts let temperature warm gradually. The intensity of cold and warm fronts has asymmetry property similar to the asymmetry property of daily mean temperature (Figure 8a);
2. When we decompose temperature tendency $\frac{\partial T}{\partial t}$ in the representative region according to Eq. (9), the horizontal advection term $-\vec{v}\cdot\nabla T$ is dominant, while the diabatic heating term $\frac{J}{c_p}$ and residual term R are ignorable. The vertical term $\left(-\omega\frac{\partial T}{\partial p}+\omega\frac{\kappa T}{p}\right)$ is not neglectable, but it does not contribute to the asymmetry property that temperature warms gradually while cools rapidly (actually it has the opposite effect) because both warm fronts and cold fronts have a positive (on average) vertical term. In other words, the asymmetric intensity of cold and warm fronts is mainly due to the asymmetry of the horizontal advection term (Figure 8a);
3. When we decompose the advection term $-\vec{v}\cdot\nabla T$ according to Eq. (10), the CAC term $\overrightarrow{\overline{v}}\cdot\nabla\overline{T}$ is ignorable, the linear term $\left(\overrightarrow{\overline{v}}\cdot\nabla T'+\overrightarrow{v'}\cdot\nabla\overline{T}\right)$ of cold and warm front are roughly equal, while the nonlinear term $\overrightarrow{v'}\cdot\nabla T'$ of cold and warm front are significantly asymmetric (Figure 8b);
4. Since $\overrightarrow{v'}\cdot\nabla T'=u'\frac{\partial T'}{\partial x}+v'\frac{\partial T'}{\partial y}$, the nonlinear advection term can be further decomposed into meridional component $v'\frac{\partial T'}{\partial y}$ and zonal component $u'\frac{\partial T'}{\partial x}$. It is clear that zonal components are roughly equal while meridional components are asymmetric (Figure 8c).

Since the nonlinear advection term involves anomaly rather than CAC variables, the asymmetric nonlinear advection between cold and warm fronts implicates that extreme cold fronts are much stronger than extreme warm fronts in north China Plain. More specifically, that is because the meridional component $v'\frac{\partial T'}{\partial y}$ of extreme cold fronts is stronger.

This result is reasonable because cold waves are quite prevalent in North China Plain. Cold waves in East Asia are often accompanied by unexpected freezes, frosts and intense northerly winds (Ding, 1990; Chen *et al.*, 2002).

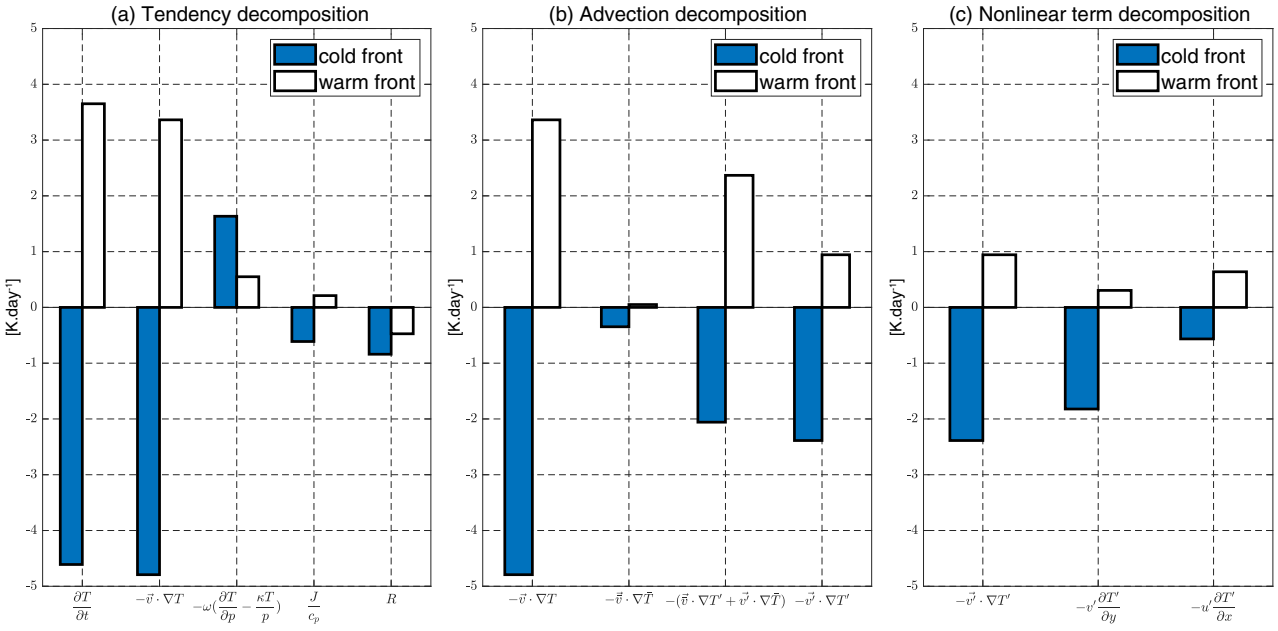

FIGURE 8 (a) Temperature tendency $\frac{\partial T}{\partial t}$ is decomposed into horizontal advection $-\vec{v}\cdot\nabla T$, vertical term $\left(-\omega\frac{\partial T}{\partial p}+\omega\frac{\kappa T}{p}\right)$, diabatic heating $\frac{J}{c_p}$ and residual term R; (b) horizontal advection $-\vec{v}\cdot\nabla T$ is decomposed into CAC term $-\overrightarrow{\overline{v}}\cdot\nabla\overline{T}$, linear advection term $-\left(\overrightarrow{\overline{v}}\cdot\nabla T'+\overrightarrow{v'}\cdot\nabla\overline{T}\right)$ and nonlinear advection term $-\vec{v'}\cdot\nabla T'$; (c) nonlinear advection term $-\vec{v'}\cdot\nabla T'$ is decomposed into zonal component and meridional component [Colour figure can be viewed at wileyonlinelibrary.com]

Therefore, it is likely that cold waves make cold fronts stronger than warm fronts by contributing to intense meridional component $v'\frac{\partial T'}{\partial y}$ of extreme cold fronts, while there is no weather system prevalent in North China Plain contributing to meridional nonlinear advection $v'\frac{\partial T'}{\partial y}$ of extreme warm fronts. The prevalence of cold waves can also explain the fact that cold fronts are much more frequent than warm fronts in North China Plain (see Figure 5).

4 | CONCLUSIONS AND DISCUSSIONS

Here, we briefly summarize our results.

1. Daily mean temperature warms gradually and cools rapidly (measure $G < 0.5$) in most parts of China (see Figure 1);
2. Temperature asymmetry is significant due to front events in some regions, and among them, we select the North China Plain as a representative region for diagnostic analysis (see Figure 7);
3. Cold fronts are more frequent than warm fronts in North China Plain (see Figure 5);
4. Cold fronts are stronger (mainly due to stronger meridional nonlinear advection) than warm fronts in North China Plain (see Figure 8).

In conclusion, the asymmetry between the frequency and intensity of cold and warm fronts contribute to the asymmetry of daily mean temperature series in North China Plain.

Furthermore, we can compare statistics in the North China Plain (the representative region in Figure 7b) with those in the Northeast China Plain (from 45° to 48°N, 121.5 to 127.5°E):

North China Plain

- G 0.43 (significant and strong, see Figure 1d);
- The correlation between front events time series and temperature asymmetry time series is −0.75 (front events and temperature asymmetry are significantly correlated, see Figure 7a);
- Cold fronts are much more frequent than warm fronts (frequency ratio for cold fronts to warm ones is nearly 10:1, see Figure 5);
- Contributions of cold fronts to temperature variations are much stronger than those of warm fronts (see Figure 8a).

Northeast China Plain

- G 0.47 (significant but weak, see Figure 1d);
- The correlation between front events time series and temperature asymmetry time series is only +0.25 (front events and temperature asymmetry are not significantly correlated, see Figure 7a);
- Cold fronts are slightly more frequent than warm fronts (frequency ratio is close to 3:2, see Figure 5);
- Cold fronts and warm fronts contribute almost equally to temperature variations (figure not shown here).

We see that the stronger the asymmetry between the frequency and intensity of cold and warm fronts is, the stronger temperature asymmetry is. Therefore, fronts do contribute to temperature asymmetry. Our results confirm the conjecture that front events contribute to temperature asymmetry. Our results are in agreement with conclusions in previous studies (Ashkenazy *et al.*, 2008; Piskala and Huth, 2020), but more direct and convincing evidences are presented here. Also, our approach can be applied easily to regions other than China.

However, we must point out that front events do not account for temperature asymmetry in all regions and at all pressure levels. For example, from Figures 1a and 5, we see that the temperature asymmetry is quite strong over the west of China, while front events are infrequent there. What's more, although not strong, there are some regions at 500 hPa pressure level (the light shading area in Figure 1f) with significant temperature asymmetry ($p < .05$ when testing the significance). Since frontal zones seldom extend to 500 hPa pressure level, the significant temperature asymmetry at 500 hPa (and higher) pressure level is caused by factors other than front events.

Besides, there are several further questions to answer. For example, why do cold fronts have stronger meridional nonlinear advection than warm fronts in North China Plain? How does the intensity of temperature asymmetry change in a warming climate? What factors cause such change? All these problems deserve further research.

ACKNOWLEDGEMENTS

The authors thank the editor and reviewers for their valuable comments and suggestions on improving our presentation. This research was supported by the National Natural Science Foundation of China through Grants (Nos. 41475048 and 41975059).

AUTHOR CONTRIBUTIONS

Heng Quan: Formal analysis; investigation; methodology; software; writing - original draft. **Wenmi Chai:** Formal analysis; investigation. **Zuntao Fu:** Conceptualization; project administration; supervision; writing-review & editing.

ORCID

Zuntao Fu https://orcid.org/0000-0001-9256-8514

REFERENCES

An, S.I. and Jin, F.F. (2004) Nonlinearity and asymmetry of ENSO. *Journal of Climate*, 17(12), 2851–2865.

Ashkenazy, Y., Feliks, Y., Gildor, H. and Tziperman, E. (2008) Asymmetry of daily temperature records. *Journal of the Atmospheric Sciences*, 65(10), 3327–3336.

Bartos, I. and Jánosi, I. (2005) Atmospheric response function over land: strong asymmetries in daily temperature fluctuations. *Geophysical Research Letters*, 32(23), 113–133.

Berry, G., Reeder, M.J. and Jakob, C. (2011) A global climatology of fronts. *Geophysical Research Letters*, 38(4), 1–5.

Burgers, G. and Stephenson, D.B. (1999) The normality of El Niño. *Geophysical Research Letters*, 26(8), 1027–1030.

Catto, J.L., Jakob, C., Berry, G. and Nicholls, N. (2012) Relating global precipitation to atmospheric fronts. *Geophysical Research Letters*, 39(10), 1–6.

Catto, J.L. and Pfahl, S. (2013) The importance of fronts for extreme precipitation. *Journal of Geophysical Research: Atmospheres*, 118(19), 10791–10801.

Chen, T.C., Yen, M.C., Huang, W.R. and Gallus, W.A. (2002) An east Asian cold surge: case study. *Monthly Weather Review*, 130(9), 2271–2290.

Cheng, J., Zhu, R., Xu, Z., Wu, J., Wang, X., Li, K., Wen, L., Yang, H. and Su, H. (2016) Impact of temperature variation between adjacent days on childhood hand, foot and mouth disease during April and July in urban and rural Hefei, China. *International Journal of Biometeorology*, 60(6), 883–890.

Cheng, J., Zhu, R., Xu, Z., Xu, X., Wang, X., Li, K. and Su, H. (2014) Temperature variation between neighboring days and mortality: a distributed lag non-linear analysis. *International Journal of Public Health*, 59(6), 923–931.

Daw, C.S., Finney, C.E.A. and Kennel, M.B. (2000) Symbolic approach for measuring temporal irreversibility. *Physical Review E*, 62(2), 1912–1921.

Dee, D.P., Uppala, S.M., Simmons, A.J., Berrisford, P., Poli, P., Kobayashi, S., Andrae, U., Balmaseda, M.A., Balsamo, G., Bauer, P., Bechtold, P., Beljaars, A.C.M., van de Berg, L., Bidlot, J., Bormann, N., Delsol, C., Dragani, R., Fuentes, M., Geer, A.J., Haimberger, L., Healy, S.B., Hersbach, H., Hólm, E. V., Isaksen, L., Kållberg, P., Köhler, M., Matricardi, M., McNally, A.P., Monge-Sanz, B.M., Morcrette, J.J., Park, B.K., Peubey, C., de Rosnay, P., Tavolato, C., Thépaut, J.N. and Vitart, F. (2011) The ERA-interim reanalysis: configuration and performance of the data assimilation system. *Quarterly Journal of the Royal Meteorological Society*, 137(656), 553–597.

Ding, Y. (1990) Build-up, air mass transformation and propagation of Siberian high and its relations to cold surge in East Asia. *Meteorology & Atmospheric Physics*, 44(1), 281–292.

Dowdy, A.J. and Catto, J.L. (2017) Extreme weather caused by concurrent cyclone, front and thunderstorm occurrences. *Scientific Reports*, 7(1), 40359.

Ehlers, C.L., James, H., Dean, P. and James, T. (1998) Low doses of ethanol reduce evidence for nonlinear structure in brain activity. *The Journal of Neuroscience*, 18(18), 7474–7486.

Guo, Y., Barnett, A.G., Yu, W., Pan, X., Ye, X., Huang, C. and Tong, S. (2011) A large change in temperature between neighbouring days increases the risk of mortality. *PLoS One*, 6(2), e16511.

Guzik, P., Piskorski, J., Krauze, T., Wykretowicz, A. and Wysocki, H. (2006) Heart rate asymmetry by Poincaré plots of RR intervals. *Biomedizinische Technik*, 51(4), 272–275.

Gyüre, B., Bartos, I. and Jánosi, I.M. (2007) Nonlinear statistics of daily temperature fluctuations reproduced in a laboratory experiment. *Physical Review E*, 76(3), 037301.

Hewson, T.D. (1998) Objective fronts. *Meteorological Applications*, 5(1), 37–65.

Hong, C.C., Li, T., Ho, L. and Kug, J.S. (2008a) Asymmetry of the Indian Ocean dipole. Part I: observational analysis. *Journal of Climate*, 21(18), 4834–4848.

Hong, C.C., Li, T. and Luo, J.J. (2008b) Asymmetry of the Indian Ocean dipole. Part II: model diagnosis. *Journal of Climate*, 21(18), 4849–4858.

Huber-Pock, F. and Kress, C. (1989) An operational model of objective frontal analysis based on ECMWF products. *Meteorology and Atmospheric Physics*, 40(4), 170–180.

Jajcay, N., Hlinka, J., Kravtsov, S., Tsonis, A.A. and Paluš, M. (2016) Time scales of the European surface air temperature variability: the role of the 7-8 year cycle. *Geophysical Research Letters*, 43(2), 902–909.

Jenkner, J., Sprenger, M., Schwenk, I., Schwierz, C., Dierer, S. and Leuenberger, D. (2010) Detection and climatology of fronts in a high-resolution model reanalysis over the Alps. *Meteorological Applications*, 17(1), 1–18.

Kang, W.Y. and Tziperman, E. (2018) The role of zonal asymmetry in the enhancement and suppression of sudden stratospheric warming variability by the madden-Julian oscillation. *Journal of Climate*, 31(6), 2399–2415.

Lacasa, L., Núñez, A., Roldán, E., Parrondo, J.M.R. and Luque, B. (2012) Time series irreversibility: a visibility graph approach. *European Physical Journal B*, 85(6), 217.

Lagerquist, R., Mcgovern, A. and Gagne, D.J. (2019) Deep learning for spatially explicit prediction of synoptic-scale fronts. *Weather and Forecasting*, 34(4), 1137–1160.

Li, T., Zhang, Y.S., Lu, E. and Wan, D.L. (2002) Relative role of dynamic and thermodynamic processes in the development of the Indian Ocean dipole: An OGCM diagnosis. *Geophysical Research Letters*, 29(23), 2110.

Luque, B., Lacasa, L., Ballesteros, F. and Luque, J. (2009) Horizontal visibility graphs: exact results for random time series. *Physical Review E*, 80(4), 46103–46103.

Mccann, D.W. and Whistler, J.P. (2001) Problems and solutions for drawing fronts objectively. *Meteorological Applications*, 8(2), 195–203.

Piskala, V. and Huth, R. (2020) Asymmetry of day-to-day temperature changes and its causes. *Theoretical and Applied Climatology*, 140(4), 683–690.

Renard, R.J. and Clarke, L.C. (1965) Experiments in numerical objective frontal analysis. *Monthly Weather Review*, 93(9), 484–497.

Schemm, S., Rudeva, I. and Simmonds, I. (2015) Extratropical fronts in the lower troposphere–global perspectives obtained from two automated methods. *Quarterly Journal of the Royal Meteorological Society*, 141(690), 1686–1698.

Steinacker, R.A. (1992) Dynamical aspects of frontal analysis. *Meteorology and Atmospheric Physics*, 48(1), 93–103.

Su, J.Z., Zhang, R.H., Li, T., Rong, X.Y., Kug, J.S. and Hong, C.C. (2010) Causes of the El Niño and La Niña amplitude asymmetry in the equatorial eastern Pacific. *Journal of Climate*, 23(3), 605–617.

Trewartha, G.T. (1954) *An Introduction to Climate*, Vol. 120, 3rd edition. New York: McGraw-Hill.

Tziperman, E. and Gildor, H. (2003) On the mid-Pleistocene transition to 100-kyr glacial cycles and the asymmetry between glaciation and deglaciation times. *Paleoceanography*, 18(1), 1001.

Vicedo-Cabrera, A.M., Bertil, F., Aurelio, T., Antonella, Z., Joel, S., Ben, A. and Antonio, G. (2015) Associations of inter- and intraday temperature change with mortality. *American Journal of Epidemiology*, 183(4), 286–293.

Wallace, J.M. and Hobbs, P.V. (2006) *Atmospheric Science: An Introductory Survey*, 2nd edition. New York: Academic Press.

Weiss, G. (1975) Time-reversibility of linear stochastic processes. *Journal of Applied Probability*, 12(4), 831–836.

Xie, F.H., Fu, Z.T., Piao, L. and Mao, J.Y. (2016) Time irreversibility of mean temperature anomaly variations over China. *Theoretical and Applied Climatology*, 123(1), 161–170.

Zhan, Z., Zhao, Y., Pang, S., Zhong, X., Wu, C. and Ding, Z. (2017) Temperature change between neighboring days and mortality in United States: a nationwide study. *Science of the Total Environment*, 584, 1152–1161.

Zhang, B.E., Xie, F.H., Fu, Z.H. and Fu, Z.T. (2019) Comparative study of multiple measures on temporal irreversibility of daily air temperature anomaly variations over China. *Physica A*, 523, 1387–1399.

Zhou, D. E. *Study on the influence of cold front on air pollution in eastern China*. PhD Thesis, Nanjing University, June 2018.

How to cite this article: Quan, H., Chai, W., & Fu, Z. (2022). Asymmetry of daily mean temperature series over China and its frontal mechanism. *International Journal of Climatology*, *42*(3), 1828–1840. https://doi.org/10.1002/joc.7338